Available online at www.sciencedirect.com

SciVerse ScienceDirect

Ceramics International 39 (2013) S549–S553

CERAMICS INTERNATIONAL

www.elsevier.com/locate/ceramint

Characterization and catalytic activity of $La_{0.6}Sr_{0.4}Co_{0.2}Fe_{0.8}O_{3-\delta}$–yttria stabilized zirconia electrospun nano-fiber as a cathode catalyst

Chen-Chia Chou[a], Chun-Feng Huang[a], Tsung-Her Yeh[b,*]

[a]*Advanced Ceramic Laboratory, Department of Mechanical Engineering, National Taiwan University of Science and Technology, Taipei, Taiwan*
[b]*Center for Thin Film Technologies and Applications, Ming Chi University of Technology, New Taipei City, Taiwan*

Available online 16 October 2012

Abstract

The influence of electrospinning parameters including polymer content and applied voltage on microstructural features of 8 mol% Y_2O_3 stabilized ZrO_2 (8YSZ) nanofiber were investigated in this work. Cathode catalyst of nano-$La_{0.6}Sr_{0.4}Co_{0.2}Fe_{0.8}O_{3-\delta}$ (LSCF) particles mixed with nano-8YSZ electrolyte fiber was coated onto 8YSZ electrolyte to study its catalytic property, compared to the powder cathode. The experimental results show that a uniform 8YSZ nanofiber of 100 nm diameter could be spun at the concentration of polyvinyl pyrrolidone (PVP) of approximately 9.89 wt% and at an applied voltage of 20 kV. The exchange current of the LSCF–8YSZ nanofiber composite cathode which is 145.06 mA/cm^2 is much better than that of the LSCF–8YSZ powder cathode which is 81.82 mA/cm^2. It is due to the increase of triple phase boundary by fiber structure to increment oxygen reduction reaction.

Keywords: B. Nanocomposites; D. ZrO_2; Fiber

1. Introduction

The combination of high specific surface area, flexibility and superior directional strength makes nanofiber a preferred material form for many applications ranging from clothing to reinforcements for aerospace structures. A number of processing techniques such as template synthesis [1], phase separation [2], self-assembly [3], electrospinning [4], etc. have been used to prepare polymer nanofibers in recent years. The electrospinning process seems to be the only method which can be further developed for mass production of one-by-one continuous nanofibers.

Compositions in the $(La_{1-x}Sr_x)_{1-z}(Co_{1-y}Fe_y)_zO_{3-\delta}$ (LSCF) system have been investigated because of their mixed conducting behavior and high electro-catalytic activity. It also has the advantage of exhibiting a greater degree of stability, both mechanically and chemically [5]. At elevated temperatures, these compositions exhibit substantial properties, making them attractive candidate materials for several important applications, including solid oxide fuel cell (SOFC) cathodes and oxygen separation membranes [6]. The high ionic conductivity makes the LSCF based materials the most promising candidates for the intermediate temperature SOFC. Zirconia is one of popular electrolyte materials employed in solid oxide fuel cells (SOFC). In particular, 8 mol% Y_2O_3–ZrO_2 (8YSZ) possesses an adequate level of oxygen-ion conductivity and exhibits higher stability in both the reducing and oxidizing environments [7].

A method for enhancement of the amount of triple phase boundary (TPB) in pure LSCF cathode should be carried out by addition of the nanofiber structure ionic conductor into cathode materials. Considering the fact that studies on this composite cathode are still lacking, we will report a comprehensive study on the microstructural characteristics and electrical properties of a modified LSCF–8YSZ cathode with nanofiber network structure in this paper. Key factors that influence the nanofiber morphology of 8YSZ, such as electric field strength and PVP concentration are studied and the possible mechanisms are discussed.

*Corresponding author. Tel.: +886 2 2908 9899x4485.
E-mail address: yeh@mail.mcut.edu.tw (T.-H. Yeh).

0272-8842/$ - see front matter © 2013 Published by Elsevier Ltd and Techna Group S.r.l.
http://dx.doi.org/10.1016/j.ceramint.2012.10.133

2. Experimental procedures

Zirconium oxychloride, $ZrOCl_2 \cdot 8H_2O$ (99.0 % purity, SHOWA, Japan) and Yttrium trinitrate hexahydrate, $Y(NO_3)_3 \cdot 6H_2O$ (99.9% purity, Alfa-Aesar, MA, USA) was used as the precursors for the synthesis of the 8 mol% yttria-stabilized zirconia (8YSZ) nanofibers. Adequate amount of $ZrOCl_2 \cdot 8H_2O$ and $Y(NO_3)_3 \cdot 6H_2O$ powders were accurately weighed and separately dissolved in minimum volume of de-ionized water by gentle stirring until clear. The polymeric solution was made by dissolving the granular polyvinyl pyrrolidone (PVP, Alfa-Aesar, MA, USA) powder in reagent grade ethanol (Fisher Chemicals, PA, USA) under constant and vigorous stirring to give the PVP solution with different concentrations.

For the electrospinning experiments, the precursor solutions (YSZ and PVP) were mixed and drawn into a 3 ml capacity Becton-Dickenson clinical syringe (Terumo, USA). An indigenously made DC power supply (20 kV max) with the high voltage system (Power 2200, Pebio, Taiwan) was used. The collector was homemade and a small 1×1 square inch of aluminum foil was attached to the back of the dish with double sided tape and the electrode was hooked to the foil. The 24-gauge stainless steel needle was positioned vertically on a clamp. The collector plate was positioned at a distance of 120 mm from the needle. This allowed the nanofibers to be collected directly onto the ceramic plate.

Fine LSCF powder and 8YSZ nanofiber were mixed thoroughly with the binder and solvent, and applied on the 8YSZ electrolyte substrates by screen printing method with the surface area of 0.38 cm^2 and fired at 1050 °C in air for 3 h to measure the exchange current density (I_0). Platinum paste (Pt-001, Sinetek, Taiwan) was painted on 8YSZ electrolyte disc to make the counter and reference electrodes. Phase identification of the specimens was analyzed using an X-ray diffractometer (M18XHF, MAC Science, Japan). The microstructural features of the modified cathodes were inspected using a scanning electron microscope (JSM-6500F, JEOL, Japan). Tafel curves of the cathodes were measured using an AC impedance analyzer (Model 1260A–1287A, Solartron, UK) with a three-point contact technique [8].

3. Results and discussion

The microstructural features of 8YSZ nanofibers were affected by different voltages as shown in Fig. 1.

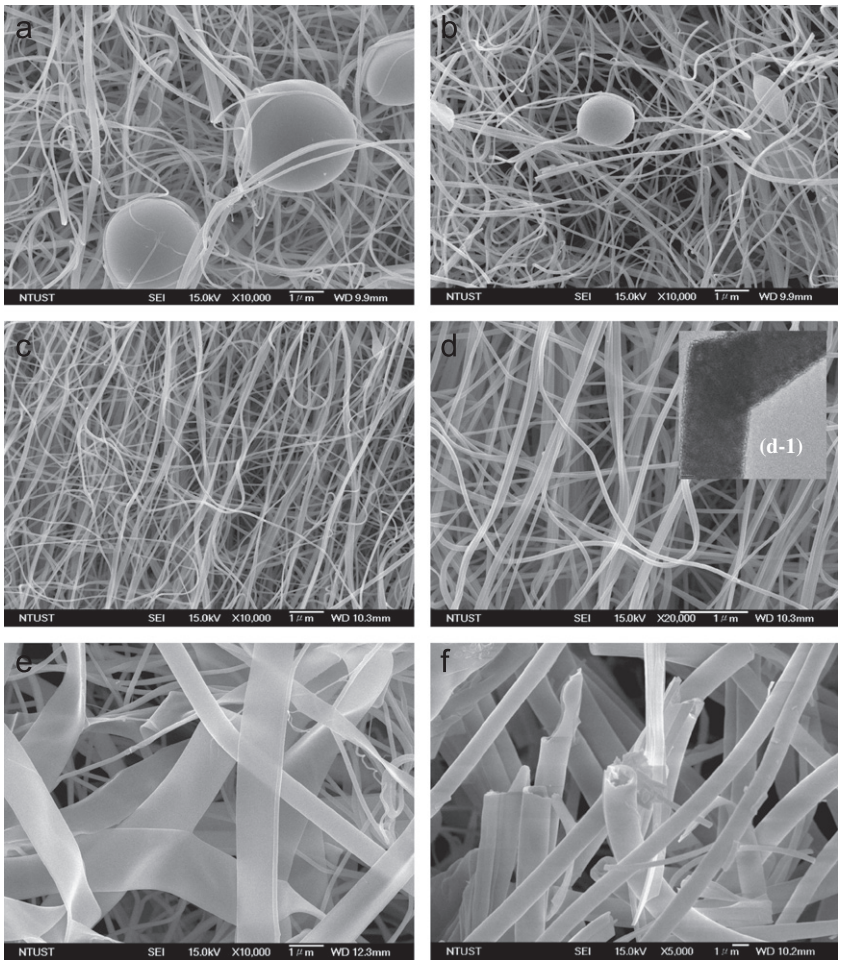

Fig. 1. SEM morphologies of 8YSZ–PVP nanofibers with different electric field strengths at (a) 10 kV, (b) 15 kV and (c) 20 kV. SEM images of 8YSZ–PVP nanofiber with the different percent weight of PVP polymer: (d) 9.89 wt% PVP (The inset: The TEM image of 8YSZ nano-fiber), (e) 12.77 wt% PVP, and (f) 15.47 wt% PVP.

The electrical forces on the jet are reduced lower than 15 kV, so that the jet behavior gradually becomes to that of an uncharged jet, and the beads are formed as shown in Fig. 1 (a and b). The diameter of beaded nanofiber at around 2 μm and 1 μm were fabricated. As the intensity of the electric field is increased from 15 kV to 20 kV, a uniform, and nano-size (~Ø100 nm) 8YSZ fiber was formed as shown in Fig. 1(c). In general, the electric field is subjected to the end of the capillary tube that contains the solution fluid held by its surface tension. This induces a charge on the surface of the liquid. Mutual charge repulsion and the contraction of the surface charges to the counter electrode cause a force directly opposite to the surface tension [9].

Fig. 1(d–f) shows a series of SEM micrographs showing the morphology changing from a beaded coating to a filamentous coating, with filamentous/beaded intermediate stages. An increase in PVP concentration from 9.89 wt% to 12.77 wt% resulted in droplets with filamentous fiber, or "flattened or ribbon-like fiber". Taylor [9] observed that in a monomeric fluid, lower viscosity resulted in the breakup of the electrically driven jet into individual droplets. The mechanism by which the flattened or ribbon-like fibers were obtained can be related to solvent evaporation during the electrospinning process. At the PVP concentration higher than 9.89 wt%, the polymer solution evidently responded to the local changes in electrostatic stresses on the surface of each droplet. These stresses deformed the individual droplets in the same way that the pendant droplet was deformed by the initial applied field. The surface morphology of the 8YSZ–PVP composite fibers (Fig. 1(d)) was smooth and uniform. The TEM image of 8YSZ fiber resulting in these small nanoparticles are mutually connected to form the 8YSZ nanofibers, indicating that the 8YSZ nanofibers were composed of nanoparticles (< 5 nm).

Fig. 1(e and f) shows the flattened or ribbon-like fiber made with higher polymer concentration. Thin polymer skin was formed on the liquid jet as a result of solvent evaporation at the jet surface, thereby resulting in a thin layer of solid skin with liquid core. As a result of atmospheric pressure, the tube collapses in tandem with solvent evaporation from the core. During the course of tube collapse, the circular cross section initially became elliptical shape, and thereafter into ribbon-like shape [10]. Small tubes formed at each edge of the ribbon and a web made from the skin connected the two tubes. Above 15.47 wt%, the mean diameters of the 8YSZ–PVP nanofibers became coarse because of the evaporation of water or decomposition of solvent. 8YSZ–PVP hollow-centered nanofibers were obtained and the length of the 8YSZ–PVP hollow nanofibers was greater than 30 μm as shown in Fig. 1(f).

Fig. 2(a) illustrates X-ray diffraction patterns of 8YSZ–PVP nanofiber after-calcined at different temperatures between 500 °C and 1500 °C for 2 hrs. The PVP polymer of 8YSZ–PVP nanofiber could be removed and the crystallinity of amorphous 8YSZ matrix could be enhanced at temperatures higher than 500 °C. The formed 8YSZ cubic nanofiber showed better crystallinity at temperatures higher than 800 °C. Uniform and small diameter 8YSZ nanofiber is found to be below 100 nm at a temperature within a range of 800–1000 °C as shown in Fig. 2(b). Nuclear chain-fiber structure formed by nucleation and growth behaviors is observed at the surface of the 8YSZ nanofiber in Fig. 2(c),

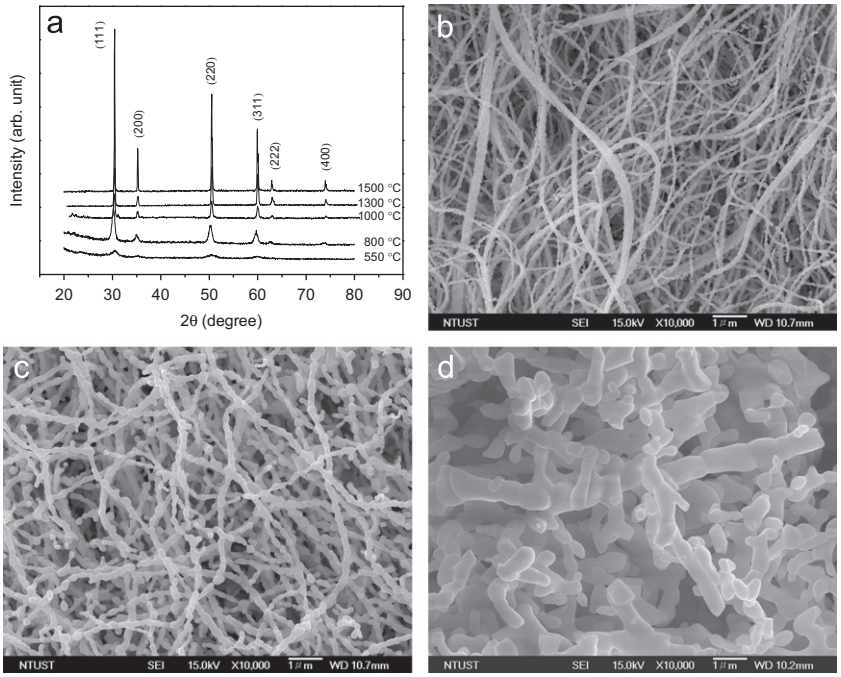

Fig. 2. (a) X-ray diffraction patterns of 8YSZ–PVP nanofiber after-calcined at different temperatures between 500 °C and 1500 °C for 2 h. Microstructural features of 8YSZ nanofibers after heated at (b) 1000 °C, (c) 1300 °C and (d) 1500 °C for 2 h.

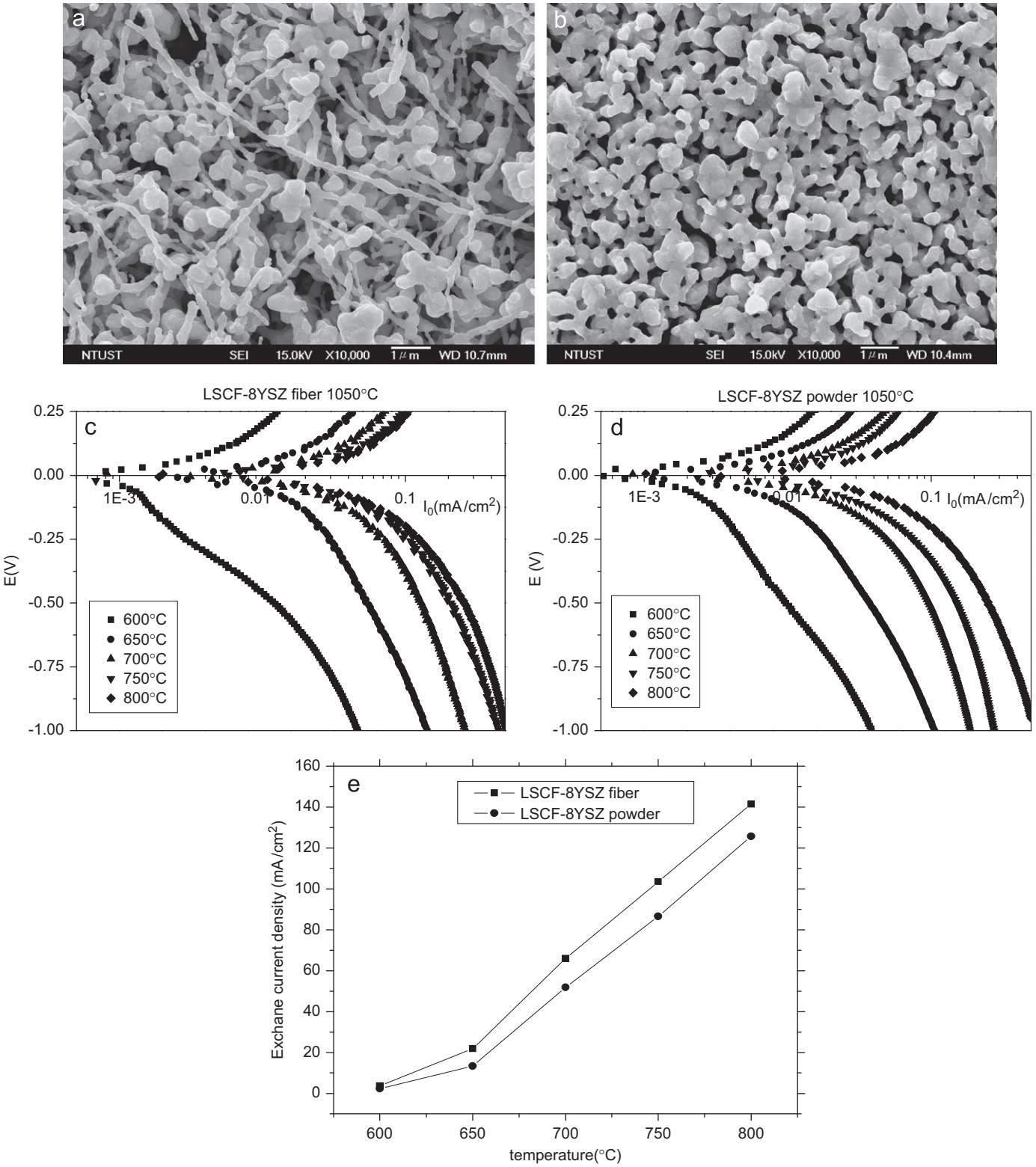

Fig. 3. (a and b) SEM images of the LSCF–8YSZ nanofiber- and LSCF–8YSZ powder-cathodes, respectively. (c and d) Tafel curves of the LSCF–8YSZ nanofiber- and LSCF–8YSZ powder-cathodes, respectively. (e) The exchange current densities of the LSCF–8YSZ nanofiber cathode and that of the LSCF–8YSZ powder cathode at different operation temperatures.

when the heating temperature was increased to 1000 °C. Fig. 2(d) shows that the morphology evolution of nano- to micro-scale fibers is strongly dependent on high temperature diffusion at heating temperature of 1500 °C. For achieving a uniform dispersion of fine LSCF nanoparticles in the 8YSZ nanofiber network structure, a three-roll miller was

employed to mix the raw materials for 30 min to provide for evenly distributing the mixture components and to provide a consistent viscosity in the resulting mixture. The LSCF–8YSZ fiber cathode (LSCF/8YSZ = 80/20 wt%) was coated onto 8YSZ electrolyte as a working electrode to measure its catalytic properties and compared to the catalytic properties of the LSCF–8YSZ powder cathode. The sintering condition for fabricating porous structure and maintaining nanofiber cathode was fixed at 1050 °C for 1 h.

$$\frac{1}{2}O_2 + 2e^- \rightarrow O^{2-}$$

The SEM image for the surface morphology of the LSCF–8YSZ fiber cathode shows uniform dispersion of fine LSCF particles in the 8YSZ nanofiber network structure to induce large amount of TPB in Fig. 3(a). The morphology of agglomerated and aggregated ceramic powders is found to decrease the amount of TPB in the LSCF–8YSZ powder cathode significantly different from that of LSCF–8YSZ nanofiber cathode as shown in Fig. 3(b). Studies on the temperature dependence of oxygen reduction reaction (ORR) on modified cathodic electrodes have been investigated in half-cells in a wide temperature range (from 600 °C to 800 °C). Fig. 3(c) illustrates the Tafel curves of the half-cells with LSCF–8YSZ nanofiber cathode measured at temperatures from 600 °C to 800 °C, the slope of linear range in the Tafel curve increases with an increase of operation temperature, implying that a faster rate of reduction at the cathode. Calculation of exchange current density in fiber based cathode with different operation temperature was carried out in a half-cell test, based on the Tafel plot analysis. The exchange current density is found to be temperature dependent. Exchange current density is an important kinetic parameter representing the electrochemical reaction rate at equilibrium. The magnitude of the exchange current density determines how rapidly the electrochemical reaction can occur. The Tafel curves of the half-cell with LSCF–8YSZ powder cathode at different temperatures from 600 °C to 800 °C are shown in Fig. 3(d). The variation in exchange current density ($\log I_0$) of the LSCF–8YSZ nanofiber cathode and that of the LSCF–8YSZ powder cathode with different temperatures in air is shown in Fig. 3(e). The O_2 reduction reaction shows a higher exchange current density on the LSCF–8YSZ nanofiber cathode (145.06 mA/cm^2) than on the LSCF–8YSZ powder cathode (81.82 mA/cm^2). The exchange current density is related to the true electrode area and to the reactant concentration (or partial pressure, for a gas), especially for ORR on the cathode in half cells. Therefore, high rate of the oxygen reduction reaction on the LSCF–8YSZ powder cathode may be due to easier migration of oxygen ion and large amount of TPB to accelerate the reaction for ionization of oxygen after substituting 8YSZ power by 8YSZ nanofiber in cathode.

4. Conclusions

This article has described the influence factors including electric field strength and the PVP concentration on the morphology of nanofiber. Uniform and polycrystalline 8YSZ nanofiber of about 100 nm diameter was prepared using a electrospinning method with the 8YSZ precursor solution of 9.89 wt% PVP and 1 M 8YSZ salt at electric field of 20 kV. SEM image for the surface morphology of the LSCF–8YSZ nanofiber cathode shows uniform dispersion of fine LSCF particles in the 8YSZ nanofiber network structure to induce a large amount of TPB. The O_2 reduction reaction exhibits a higher exchange current density on the LSCF–8YSZ nanofiber cathode (145.06 mA/cm^2) than on the LSCF–8YSZ powder cathode (81.82 mA/cm^2) at 800 °C. This is attributed to the increase of the amount of TPB and decrease of the activation energy for oxygen ion migration by modifying high length/diameter ionic conductor in cathode materials.

Acknowledgments

Financial support from the National Science Council of Taiwan, Republic of China through Project no. NSC 99-2221-E-011-042-MY3 is gratefully acknowledged by the authors.

References

[1] L. Eng, S. Li, H. Li, J. Zhai, Y. Song, L. Jiang, Super-hydrophobic surface of aligned polyacrylonitrile nanofibers, Angewandte Chemie International Edition 41 (7) (2002) 1221–1223.
[2] P.X. Ma, R. Zhang, Synthetic nano-scale fibrous extracellular matrix, Journal of Biomedical Materials Research 46 (1999) 60–72.
[3] G.J. Liu, J.F. Ding, L.J. Qiao, A. Guo, B.P. Dymov, J.T. Gleeson, Polystyrene-block-poly (2-cinnamoylethyl methacrylate) nanofibers—preparation, characterization, and liquid crystalline properties, Chemistry—A European Journal 5 (1999) 2740–2749.
[4] J.M. Deitzel, J. Kleinmeyer, J.K. Hirvonen, T.N.C. Beck, Controlled deposition of electrospun poly(ethylene oxide) fibers, Polymer 42 (8) (2001) 163–170.
[5] S.C. Singhal, Advances in solid oxide fuel cell technology, Solid State Ionics 135 (2000) 305–313.
[6] Y. Teraoka, H. Zhang, K. Okamoto, N. Yamazoe, Mixed ionic-electronic conductivity of $La_{1-x}Sr_xCo_{1-y}Fe_yO_{3-\delta}$ perovskite-type oxides, Materials Research Bulletin 23 (1988) 51–58.
[7] A. Nakamura, J.B. Wagner Jr., The electrical conductivity of yttria-stabilized zirconia prepared by precipitation from inorganic aqueous solutions, Journal of The Electrochemical Society 133 (1986) 1542.
[8] S.B. Adler, Limitations of charge-transfer models for mixed-conducting oxygen electrodes, Solid State Ionics 135 (2000) 603–612.
[9] S.G. Taylor, Electrically driven jets, Proceedings of the Royal Society of London A 313 (1969) 453–475.
[10] S. Koombhongse, W. Liu, D.H. Reneker, Flat polymer ribbons and other shapes by electrospinning, Journal of Polymer Science Part B: Polymer Physics 39 (21) (2001) 2598–2606.